

# RSC Advances



This is an *Accepted Manuscript*, which has been through the Royal Society of Chemistry peer review process and has been accepted for publication.

*Accepted Manuscripts* are published online shortly after acceptance, before technical editing, formatting and proof reading. Using this free service, authors can make their results available to the community, in citable form, before we publish the edited article. This *Accepted Manuscript* will be replaced by the edited, formatted and paginated article as soon as this is available.

You can find more information about *Accepted Manuscripts* in the [Information for Authors](#).

Please note that technical editing may introduce minor changes to the text and/or graphics, which may alter content. The journal's standard [Terms & Conditions](#) and the [Ethical guidelines](#) still apply. In no event shall the Royal Society of Chemistry be held responsible for any errors or omissions in this *Accepted Manuscript* or any consequences arising from the use of any information it contains.

# **SiO<sub>2</sub>-confined silicon/carbon nanofiber composites as anode for lithium-ion batteries**

**Mahmut Dirican<sup>a,b</sup>, Yao Lu<sup>a</sup>, Kun Fu<sup>a</sup>, Huseyin Kizil<sup>b</sup>, and Xiangwu Zhang<sup>a,\*</sup>**

<sup>a</sup>Fiber and Polymer Science Program, Department of Textile Engineering, Chemistry and Science, North Carolina State University, Raleigh, NC 27695-8301, USA

<sup>b</sup>Nano-Science and Nano-Engineering Program, Graduate School of Science, Engineering and Technology, Istanbul Technical University, Istanbul 34469, Turkey

\*Corresponding author: Xiangwu Zhang

Tel: 919-515-6547; Fax: 919-515-6532; E-mail: xiangwu\_zhang@ncsu.edu

## Abstract

Because of its ultra-high theoretical capacity ( $4200 \text{ mAh g}^{-1}$ ), Si is considered as the most promising anode material candidate for next-generation high-energy lithium-ion batteries. However, the practical use of Si based anodes is constrained by the high volume change (up to 400%) of Si active material during cycling. Intensive volume change of Si causes severe pulverization, loss of electrical contact between Si particles and carbon current collector, and unstable SEI formation on the electrode surface. Herein, we introduce nanoscale silica-coated silicon/carbon (Si@C-SiO<sub>2</sub>) nanofiber composites that can maintain their structural stability during repeated cycling. Results indicated that nanoscale SiO<sub>2</sub> coating of Si@C nanofibers helped preserve the Si particles within the nanofiber structure, resulting in stable solid electrolyte interphase formation and improved cycling performance. Electrochemical performance results showed that Si@C-SiO<sub>2</sub> nanofiber composite anodes had good capacity retention of 89.8% and high coulombic efficiency of 97.2% at the 50th cycle. It is, therefore, demonstrated that nanoscale SiO<sub>2</sub> coating is an effective method to improve the electrochemical performance of Si@C nanofiber composite anodes.

**Keywords:** Lithium-ion battery; Carbon nanofiber; Silicon; Nanoscale SiO<sub>2</sub> coating; Capacity retention; Coulombic efficiency

## 1. Introduction

Among existing rechargeable battery technologies, lithium-ion batteries draw great attention in recent years because of their superior properties, including high energy density, durable cycle life and good power performance.<sup>1, 2</sup> With recent improvements in technologies of electric vehicles and portable electronic devices, development of high-capacity electrode materials for high-energy lithium-ion batteries becomes critically important to meet their energy requirements.<sup>3-5</sup> For most current commercial lithium-ion batteries, graphitic materials are used in the anode because of their low cost and long cycling performance. However, graphitic anode materials are not capable of meeting the ever-growing capacity requirements of future portable electronics and electric vehicles because of their low specific capacity of 372 mAh g<sup>-1</sup>.<sup>6, 7</sup> On the other hand, lithium storage capacities of alloy-type anodes (e.g., silicon, tin, germanium, and their oxides) are much higher than those of commercially-used intercalation-type graphite anodes.

Among all alloy-type anodes, Si provides the highest theoretical specific capacity of 4200 mAh g<sup>-1</sup>. Because of its ultra-high theoretical capacity, Si is considered as the most promising candidate for next-generation high-energy lithium-ion batteries.<sup>8, 9</sup> However, similar to other alloy-type anode materials, the insertion of lithium ions into Si during charge and discharge causes high volumetric change (up to 400%), which results in intense pulverization of active Si material and significant loss of electrical contact between Si particles and carbon conductor. In addition, high volume expansion and intense pulverization of active Si particles triggers extra electrolyte consumption on the fresh surface of Si, leading to unstable solid-electrolyte-interphase (SEI) film formation.<sup>10, 11</sup> These drawbacks result in the severe capacity fading of Si-based anodes during repetitive lithiation and delithiation processes.<sup>12</sup> Reducing the size of Si

particles into the nanoscale range and embedding them into carbon structures are some of the accepted effective methods for minimizing the volume expansion problem of Si-based anodes. Nano-sized Si/carbon (Si/C) composite anodes combine the advantageous properties of Si (high capacity) and carbon (excellent electronic conductivity and structural stability).<sup>13, 14</sup>

Carbon nanofibers are one of the best options for hosting active Si due to their high electronic conductivity, large surface area, and good electrochemical stability.<sup>15</sup> However, electrochemical performance results of the reported Si/C nanofiber composites are well below the expected performance due to direct exposure of Si nanoparticles with the electrolyte on the fiber surfaces which leads to heavy SEI formation.<sup>16, 17</sup> The exposed Si nanoparticles could also be detached from the nanofiber surfaces during the repetitive cycling processes. To eliminate the aforementioned problems, Fu, et al., and Dirican, et al., introduced an additional nanoscale disordered carbon layer onto the surface of Si@C nanofibers by chemical vapor deposition (CVD) technique to prevent direct exposure of the Si nanoparticles with the electrolyte solution and increase the mechanical bonding strength between the Si nanoparticles and carbon nanofiber matrix.<sup>15, 18</sup> With the additional protective layer, not only stable SEI is formed but also the detachment of Si nanoparticles from the nanofiber surfaces can be prevented. Confinement of the Si nanoparticles can also be ensured by using an easy and low-cost sol-gel method to form nanoscale amorphous SiO<sub>2</sub> coating on Si@C nanofibers. Similar to nanoscale carbon coating, nanoscale SiO<sub>2</sub> coating can lead to stable SEI formation on coated nanofiber surfaces and increased mechanical bonding between Si nanoparticles and carbon nanofiber matrix.

In this study, we report nanoscale SiO<sub>2</sub> coated Si@C (Si@C-SiO<sub>2</sub>) nanofiber composites as high-energy anodes for lithium-ion batteries. We introduced a feasible method to improve the electrochemical performance of previously reported Si@C nanofiber composite electrodes. The

main target of this study is to propose a simple, but effective approach for the confinement of Si nanoparticles inside the Si@C nanofiber composite electrodes. Si@C nanofibers were produced by simple electrospinning and subsequent heat treatment processes. The resultant Si@C nanofibers were coated with thin amorphous SiO<sub>2</sub> layers by using sol-gel TEOS solution to achieve further improvement on the cycling performance of the composite anodes. Nanoscale SiO<sub>2</sub> coating helped maintain the Si nanoparticles within the nanofiber structure and stabilize the SEI formation, resulting in improved cycling performance. Electrochemical performance results show that Si@C-SiO<sub>2</sub> nanofiber composite anodes exhibit capacity retention of 89.8% and coulombic efficiency of 97.2% after 50th cycles. Although better electrochemical performance (e.g., higher capacity retention or higher coulombic efficiency) has been reported in the literature,<sup>14, 19</sup> this work does present an easy and versatile approach for improving the electrochemical performance of previously reported Si@C nanofiber composite electrodes. Nevertheless, future study can be conducted to refine the structure of Si@C-SiO<sub>2</sub> nanofiber composite and further improve their electrochemical performance. In addition, the method used in this work can be applied to most of the previously reported Si/C based composite anodes to improve their performance.

## 2. Experimental

### 2.1. Nanofiber preparation

Tetraethyl orthosilicate (TEOS, 99%), polyacrylonitrile (PAN,  $M_w = 150,000$  g/mol), *N,N*-dimethylformamide (DMF), ammonium hydroxide solution (NH<sub>4</sub>OH, 28-30%), and ethanol were purchased from Sigma-Aldrich. Si nanoparticles (diameter: 30-50 nm) were purchased from

Nanostructures & Amorphous Materials, Incorporated. All chemicals were used without further purification.

Figure 1 schematically illustrates the entire fabrication approach of electrospun Si@PAN nanofibers, Si@C nanofibers, and Si@C-SiO<sub>2</sub> nanofibers. For the preparation of Si@PAN nanofibers, PAN (8 wt%) was first dissolved in DMF at 60 °C and mechanically stirred for 24 h. Si nanoparticles (20 wt% with respect to PAN) were then added into the as-prepared PAN/DMF solution and stirred at room temperature for 24 h, followed by ultrasonic treatment for 1 h to obtain a homogenous dispersion. The as-prepared Si/PAN dispersion was then electrospun into Si@PAN nanofibers with a flow rate of 0.75 ml/h, a voltage of 16 kV, and a tip-to-collector distance of 25 cm. Si@C nanofiber composites were prepared from Si@PAN nanofibers through stabilization in air environment at 280 °C for 5.5 h with a heating rate of 5 °C min<sup>-1</sup>, followed by carbonization at 700 °C for 2 h in argon atmosphere with a heating rate of 2 °C min<sup>-1</sup>, during which PAN was pyrolyzed to carbon.

For the preparation of Si@C-SiO<sub>2</sub> nanofiber composites, the as-prepared Si@C nanofibers were coated with nanoscale SiO<sub>2</sub> by using a sol-gel TEOS solution. The sol-gel TEOS solution was prepared by adding 3 ml ammonium hydroxide into a mixture of 125 ml ethanol and 30 ml water, followed by the addition of 2.4 g TEOS dropwise under vigorous stirring. The reaction was left at room temperature under vigorous stirring for 30 minutes. During the synthesis of Si@C-SiO<sub>2</sub> nanofiber composites, 100 mg Si@C nanofibers were immersed into the as-prepared sol-gel TEOS solution and treated for different duration times. Solution treatment time was varied from 0.5 h, 1 h to 2 h to investigate its effect on electrochemical performance. After solution treatment, the Si@C-SiO<sub>2</sub> nanofiber composites were first dried in vacuum oven and later washed with deionized water for three times.

## 2.2. Structure characterization

The morphology of nanofiber composites was examined by field emission scanning electron microscope (FE-SEM, FEI Verios 460 L) and scanning transmission electron microscope (STEM, JEOL 2000FX). The structure of composite nanofibers was investigated by Fourier transform infrared spectroscopy (FTIR, Nicolet Nexus 470), wide angle X-ray diffraction (WAXD, Rigaku Smartlab), and Renishaw Raman microscope. Compositions of the nanofiber composites were examined by elemental analysis (Perkin Elmer 2400 Series II CHNS/O Elemental Analyzer).

## 2.3. Electrochemical evaluation

The electrochemical properties of Si@C-SiO<sub>2</sub> nanofiber composites were tested using CR 2032-type coin cells. The working electrodes were prepared by mixing 70 wt% grounded nanofiber composites with 20 wt% carbon black and 10 wt% sodium alginate binder. The slurry of each sample was coated on copper foil substrates and vacuum-dried for 12 h at 80 °C. The average mass loading of the electrodes used in this study was 1.2 mg cm<sup>-2</sup>. Lithium ribbon (99.9%, Aldrich) was used as the counter electrode and Celgard 2400 membrane was used as the separator. The electrolyte consisted of a 1 M solution of LiPF<sub>6</sub> dissolved in ethylene carbonate (EC) + dimethyl carbonate (DMC) + diethyl carbonate (DEC) (1:1:1 by volume, MTI Corporation). Coin cells were assembled in a high-purity argon-filled glove box. The electrochemical performance was investigated by galvanostatic charge-discharge experiments at a constant current density of 100 mA g<sup>-1</sup> (around C/10) with cut-off potentials between of 0.01 and 2.00 V on a LAND-CT 2001A battery test system.

### 3. Results and Discussion

#### 3.1. Morphology and structure

Figure 1 shows schematically the fabrication approach of Si@PAN nanofibers, Si@C nanofibers, and Si@C-SiO<sub>2</sub> nanofibers. Fabrication process of these nanofiber composites composed of three steps: electrospinning of Si/PAN solution into Si@PAN nanofibers, stabilization and carbonization of electrospun nanofibers to obtain Si@C nanofibers, and SiO<sub>2</sub> coating of Si@C nanofibers to form Si@C-SiO<sub>2</sub> nanofibers. Compositions of the nanofiber composites were calculated based on the elemental analysis data. Elemental analysis results revealed that Si@C nanofibers contained 24.05% Si, 10.30% SiO<sub>2</sub>, and 65.65% C. The SiO<sub>2</sub> component of Si@C nanofibers might come from the surface oxidation of Si nanoparticles. The Si@C-SiO<sub>2</sub> nanofiber composite with 0.5 h coating time had 22.80% Si, 14.94% SiO<sub>2</sub>, and 62.26% C. Here, the SiO<sub>2</sub> content was the sum of SiO<sub>2</sub> coating layer on the fiber surface and the oxidized SiO<sub>2</sub> on Si nanoparticles. With increase in coating time, the SiO<sub>2</sub> content increased. The Si@C-SiO<sub>2</sub> nanofiber composite with 1 h coating time was composed of 22.40% Si, 16.45% SiO<sub>2</sub>, and 61.15% C, and the Si@C-SiO<sub>2</sub> nanofiber composite with 2 h coating time contained 21.98% Si, 17.97% SiO<sub>2</sub>, and 60.05% C.

The morphology of Si@C nanofibers and Si@C-SiO<sub>2</sub> nanofibers with different coating times was examined by using SEM, as shown in Figure 2. Continuous nanofibers were observed from the SEM image of Si@C nanofibers (Figure 2A). From Figures 2B, C and D, it is seen that the surface morphologies of Si@C-SiO<sub>2</sub> nanofibers were similar to that of Si@C nanofibers. Si nanoparticles were dispersed throughout the carbon nanofiber matrices with some particles agglomerated on the nanofiber surfaces. From the SEM images of Si@C-SiO<sub>2</sub> nanofibers, the

presence of SiO<sub>2</sub> coating layers was not apparent due to limited image resolution. To clearly observe the thin SiO<sub>2</sub> layers, TEM observation was carried out, as discussed below.

Figure 3 shows TEM images of Si/C and Si@C-SiO<sub>2</sub> nanofibers. TEM images show that for all four nanofiber composites, the Si nanoparticles were not completely confined in the nanofiber matrices and some nanoparticles were agglomerated and located on nanofiber surfaces, which agreed with the SEM observation in Figure 2. For the pristine Si@C nanofibers, no SiO<sub>2</sub> coating was observed on the exposed Si nanoparticles (Figure 3A). On the other hand, Si@C-SiO<sub>2</sub> nanofibers prepared with 0.5 h, 1 h, and 2 h SiO<sub>2</sub> coating times exhibited amorphous SiO<sub>2</sub> coatings on the Si nanoparticle surfaces (Figures 3B, C, and D).

High-magnification TEM images of nanofiber composites are presented in Figure 4 to further illustrate the amorphous SiO<sub>2</sub> coating layers on the Si@C-SiO<sub>2</sub> nanofiber composites. For the pristine Si@C nanofiber composite, no SiO<sub>2</sub> coating was observed on the nanofiber surface (Figure 4A). However, nanoscale amorphous SiO<sub>2</sub> layers were clearly shown on the surfaces of Si@C-SiO<sub>2</sub> nanofiber composites. The thickness of the SiO<sub>2</sub> coating layers increased, on average, from 7 nm, 10 nm, to 13 nm, respectively, when the SiO<sub>2</sub> coating time increased from 0.5 h, 1 h, to 2 h. These nanoscale SiO<sub>2</sub> layers were important for stable SEI formation on the active materials during the repetitive electrode reactions, especially for the Si nanoparticles exposed on the carbon nanofiber surfaces.

Figure 5 shows the FTIR spectra of Si@C and Si@C-SiO<sub>2</sub> nanofiber composites. For all nanofiber composites, two characteristic peaks were indexed at around 1280 cm<sup>-1</sup> and 1590 cm<sup>-1</sup>, which were attributed to the C–C and C=C stretch bonds, respectively.<sup>20</sup> FTIR spectra of Si@C and Si@C-SiO<sub>2</sub> nanofiber composites also showed a characteristic SiO<sub>2</sub> side peak at around 1100

$\text{cm}^{-1}$ , corresponding to the symmetric stretching, asymmetrical stretching, and bending vibrations in Si-O-Si bonds.<sup>21</sup> Since the pristine Si@C nanofiber composite do not have SiO<sub>2</sub> coating, the observed side peak at around 1100  $\text{cm}^{-1}$  was weaker than those of Si@C-SiO<sub>2</sub> nanofiber composites. The presence of side peak at around 1100  $\text{cm}^{-1}$  for Si@C nanofibers may be ascribed to the partial oxidation of Si nanoparticles.

The X-ray diffraction (XRD) patterns of Si@C and Si@C-SiO<sub>2</sub> nanofiber composites are shown in Figure 6. For all nanofiber composites, similar diffraction peaks were indexed. Diffraction peaks at  $2\theta$  of about 29°, 47°, 56°, 69°, 76°, and 88° represented the (111), (220), (311), (400), (331), and (422) planes of Si crystals in carbon nanofiber composites, respectively.<sup>22,23</sup> In addition, as shown in Figure 6, all nanofiber composites showed a broad and weak diffraction peak at around  $2\theta = 25^\circ$ , which could be indexed as the (002) planes of disordered carbon structure, indicating the amorphous nature of the carbon nanofiber matrix.<sup>15,16</sup>

The structural evolution of the nanofiber composites was also investigated by Raman spectroscopy. Figure 7 shows the Raman spectra of Si@C and Si@C-SiO<sub>2</sub> nanofiber composites. For all nanofiber composites, the characteristic carbon peaks of D-band (1360  $\text{cm}^{-1}$ ), indicating the disordered sp<sup>2</sup> phase, and G-band (1582  $\text{cm}^{-1}$ ), representing the in-plane stretching vibration mode of E<sub>2g</sub> graphite, were indexed.<sup>24,25</sup> From Figure 7, it was also seen that due to the presence of Si nanoparticles, these nanofiber composites exhibited a Si peak at around 522  $\text{cm}^{-1}$ , which is a position for the transverse optical phonon.<sup>26</sup> In addition, Si@C-SiO<sub>2</sub> nanofiber composites with different SiO<sub>2</sub> coating times had a broad and weak peak at around 900  $\text{cm}^{-1}$ , representing the SiO<sub>2</sub> component of the Si@C-SiO<sub>2</sub> nanofiber composites.<sup>27</sup>

### 3.2. Electrochemical performance

Galvanostatic charge-discharge tests were conducted between 0.01 and 2.0 V at a constant current density of 100 mA g<sup>-1</sup> to evaluate the electrochemical performance of the nanofiber composite anodes. The specific capacities of all nanofiber composite electrodes were calculated based on the total mass of nanofiber composites by including Si, C, and SiO<sub>2</sub> coating if any. Figure 8 represents the first, second and tenth cycle of the galvanostatic charge-discharge profiles of Si@C and Si@C-SiO<sub>2</sub> nanofiber composites. The first-cycle discharge capacities were 1506, 1570, 1567, and 1481 mAh g<sup>-1</sup>, respectively, for Si@C nanofiber composite and Si@C-SiO<sub>2</sub> nanofiber composites with different coating times: 0.5 h, 1 h, and 2 h. For the Si@C nanofiber composite, the initial discharge and charge capacities reached 1506 and 1138 mAh g<sup>-1</sup>, respectively, with a coulombic efficiency of 75.6%. At the 10th cycle, the discharge and charge capacities changed to 1193 mAh g<sup>-1</sup> and 1168 mAh g<sup>-1</sup>, with a coulombic efficiency of 97.9% (Figure 8A). On the other hand, the initial discharge and charge capacities of Si@C-SiO<sub>2</sub> nanofiber composite with 0.5 h coating time were 1570 and 1222 mAh g<sup>-1</sup>, respectively, with a coulombic efficiency of 77.8%. At the 10th cycle, the discharge and charge capacities of Si@C-SiO<sub>2</sub> nanofiber composite with 0.5 h coating time reduced to 1181 mAh g<sup>-1</sup> and 1157 mAh g<sup>-1</sup>, with a coulombic efficiency of 98.0% (Figure 8B). Initial charge and discharge capacities of Si@C-SiO<sub>2</sub> nanofiber composite with 1 h coating time were 1567 and 1215 mAh g<sup>-1</sup>, respectively, with a coulombic efficiency of 77.5%. At the 10th cycle, the discharge and charge capacities of Si@C-SiO<sub>2</sub> nanofiber composite with 1 h coating time reduced to 1078 mAh g<sup>-1</sup> and 1058 mAh g<sup>-1</sup>, with a coulombic efficiency of 98.2% (Figure 8C). For the Si@C-SiO<sub>2</sub> nanofiber composite with 2 h coating time, the initial discharge and charge capacities reached 1481 and 1183 mAh g<sup>-1</sup>, respectively, with a coulombic efficiency of 79.8%. At the 10th cycle, the discharge and charge capacities reduced to 993 mAh g<sup>-1</sup> and 957 mAh g<sup>-1</sup>, with a coulombic

efficiency of 96.3% (Figure 8D). These results show that for both first and tenth cycles, the coulombic efficiencies of Si@C-SiO<sub>2</sub> nanofiber composites with 0.5 and 1 h coating times were better than those of Si@C nanofiber composite. From Figure 8, it is also seen that there are two voltage plateaus, indexed at 0.7 V and 0.2 V, respectively, in the first-cycle discharge curve of Si@C-SiO<sub>2</sub> nanofiber composites. The plateau at 0.7 V was associated with the electrolyte decomposition and SEI formation while the plateau at 0.2 V was ascribed to electrochemical reactions between lithium ions and the SiO<sub>2</sub> ingredient of the composite nanofibers. During the initial lithiation process, SiO<sub>2</sub> might be reduced to electrochemically inactive Li<sub>2</sub>O and Li<sub>4</sub>SiO<sub>4</sub>.<sup>28, 29</sup> On the other hand, without the presence of SiO<sub>2</sub>, the Si@C nanofiber composite did not exhibit the plateau at 0.2 V. When comparing the charge-discharge profiles of Si@C-SiO<sub>2</sub> composites with different coating times, it can be found that the voltage plateau under the curve of the electrolyte reduction/degradation stage at 0.7 V was shortened with increasing SiO<sub>2</sub> coating time, indicating that less electrolyte participated in the formation of SEI due to the presence of SiO<sub>2</sub> coating on the nanofiber surface.<sup>15</sup>

The cycling performance of Si@C and Si@C-SiO<sub>2</sub> nanofiber composites was compared in Figure 9. Capacity retention and coulombic efficiency of the Si/C nanofiber composite at the 50th cycle were around 42.5% and 95.9%, respectively, indicating unstable cycling behavior. On the other hand, relatively stable cycling performance was achieved for the Si@C-SiO<sub>2</sub> nanofiber composite with 0.5 h coating time. At the 50th cycle, the capacity retention and coulombic efficiency of Si@C-SiO<sub>2</sub> nanofiber composite with 0.5 h coating time were around 89.8% and 97.2%, respectively. Compared to Si@C nanofiber composite, Si@C-SiO<sub>2</sub> nanofiber composite with 0.5 h coating time showed much slower capacity decay in 50 cycles. This result demonstrated that the nanoscale SiO<sub>2</sub> coating enhanced the confinement of Si nanoparticles on

nanofiber surfaces and helped maintain the structural integrity of the electrode during the cycling process. Furthermore, during the initial lithiation process, the amorphous  $\text{SiO}_2$  structure might be reduced to  $\text{Li}_2\text{O}$  and  $\text{Li}_4\text{SiO}_4$ , which could help accommodate the volume expansion caused by the alloying of Si nanoparticles with Li, and thereby increased the cycling stability by minimizing the pulverization of the active Si material and the loss of electrical contact between Si nanoparticles and the carbon nanofiber matrix.<sup>28, 29</sup>  $\text{SiO}_2$  coating layer also supported more stable SEI formation by preventing direct contact of the electrolyte with the active Si material. Similar effects of nanoscale  $\text{SiO}_2$  coating have been reported by Wu, et al., who obtained improved cycling stability for ion-permeable nanoscale  $\text{SiO}_2$  surrounded silicon nanotube anodes.<sup>30</sup> From Figure 9, it is also seen that the cycling performance of Si@C- $\text{SiO}_2$  nanofiber composites was worsened while increasing  $\text{SiO}_2$  coating time to 1 h or 2 h. The capacity retention and coulombic efficiency of Si@C- $\text{SiO}_2$  nanofiber composite with 1 h coating time was around 75.0% and 97.8%, respectively, at the 50th cycle. For the Si@C- $\text{SiO}_2$  nanofiber composite with 2 h coating time, the capacity retention and coulombic efficiency were only around 64.5% and 96.2%, respectively, at the 50th cycle. Therefore, to achieve the enhanced cycling performance, it is very crucial to select an appropriate  $\text{SiO}_2$  coating thickness for Si@C- $\text{SiO}_2$  nanofiber composites. The cycling performance was affected by the easiness of Li-ion diffusion through the  $\text{SiO}_2$  and SEI layer formed on the nanofiber surface. The fast capacity fading of Si@C- $\text{SiO}_2$  nanofiber composites with 1 and 2 h coating times might be caused by the hindered Li-ion insertion/deinsertion during cycling due to their relatively thick  $\text{SiO}_2$  coating layers. Similar results were reported for nano Si powder electrodes with different oxide layer thicknesses by Yu, et al.<sup>31</sup> In many reported studies, Si based anodes were evaluated with a cutoff voltage window of 0.01 and 1.0 V. To put our results into perspective, we tested our

electrodes between 0.01 and 1.0 V at a constant current density of  $100 \text{ mA g}^{-1}$ , and the measured coulombic efficiencies are shown in Figure 10. Results revealed that the coulombic efficiencies of the nanofiber composites in a cutoff voltage window of 0.01 and 1.0 V were quite similar to those tested with a cutoff voltage window of 0.01 and 2.0 V.

The Si@C-SiO<sub>2</sub> nanofiber composite with 0.5 h coating time showed the best cycling performance among all the studied nanofiber composites. Therefore, this composite was further investigated for its rate capability under various current densities, as shown in Figure 11. It was observed that the charge capacities were around 1177, 1028, 873, and 683  $\text{mAh g}^{-1}$ , respectively, at current densities of 100, 200, 400, and 800  $\text{mA g}^{-1}$ . The coulombic efficiency remained relatively constant as the current density increased. In addition, the charge capacity reached 1052  $\text{mAh g}^{-1}$  when the current density returned to 100  $\text{mA g}^{-1}$  after ongoing cycles at higher current densities. This charge capacity (1052  $\text{mAh g}^{-1}$ ) was very close to initial charge capacity (1177  $\text{mAh g}^{-1}$ ), demonstrating the good rate capability of the Si@C-SiO<sub>2</sub> nanofiber composite.

Electrochemically tested cells were disassembled after 50 cycles to analyze the surface morphology change of Si@C and Si@C-SiO<sub>2</sub> nanofiber composites using TEM (Figure 12). Before TEM observation, the cycled electrodes were washed by HCl to remove SEI. Due to the repeated large volume expansion and contraction of Si nanoparticles, the Si@C nanofiber composite suffered major structural deterioration during the cycling and Si nanoparticles fell off from the carbon matrix, causing irreversible structure damage (Figure 12A). On the other hand, in Si@C-SiO<sub>2</sub> nanofiber composites, most of the Si nanoparticles were maintained and encapsulated inside the nanofiber matrix after cycling, without catastrophic structural damage to the nanofiber surfaces (Figures 12B, C, and D). Results demonstrated that the SiO<sub>2</sub> coating helped restrict Si nanoparticles in carbon matrix during the repetitive cycles.

## 4. Conclusions

Nanoscale SiO<sub>2</sub> coating of Si@C nanofiber composites were performed to prevent direct exposure of the Si nanoparticles with the electrolyte solution and increase the mechanical bonding strength between the Si nanoparticles and carbon nanofiber matrix. Results demonstrated that nanoscale SiO<sub>2</sub> coating of Si@C nanofibers helped maintain the Si nanoparticles within the nanofiber structure and stabilize the SEI formation on the electrode surface, resulting in improved cycling performance. Electrochemical performance results showed that the Si@C-SiO<sub>2</sub> nanofiber composite anode with 0.5 h coating time exhibited good capacity retention of 89.8% and high coulombic efficiency of 97.2% at the 50th cycle. It is, therefore, demonstrated that Si@C-SiO<sub>2</sub> nanofiber composites are promising anode material candidate for next-generation high-energy lithium-ion batteries.

## References

1. H. Wu, G. Zheng, N. Liu, T. J. Carney, Y. Yang and Y. Cui, *Nano Lett.*, 2012, 12, 904-909.
2. X. Zhang, L. Ji, O. Toprakci, Y. Liang and M. Alcoutlabi, *Polym. Rev.*, 2011, 51, 239-264.
3. H. Gwon, H.-S. Kim, K. U. Lee, D.-H. Seo, Y. C. Park, Y.-S. Lee, B. T. Ahn and K. Kang, *Energy Environ. Sci.*, 2011, 4, 1277-1283.
4. J.-Z. Wang, C. Zhong, S.-L. Chou and H.-K. Liu, *Electrochem. Commun.*, 2010, 12, 1467-1470.
5. M. Dirican, M. Yanilmaz, K. Fu, Y. Lu, H. Kizil and X. Zhang, *J. Power Sources*, 2014.
6. B. S. Lee, S. B. Son, J. H. Seo, K. M. Park, G. Lee, S. H. Lee, K. H. Oh, J. P. Ahn and W. R. Yu, *Nanoscale*, 2013, 5, 4790-4796.
7. L. Ji, Z. Lin, R. Zhou, Q. Shi, O. Toprakci, A. J. Medford, C. R. Millns and X. Zhang, *Electrochim. Acta*, 2010, 55, 1605-1611.
8. T. H. Hwang, Y. M. Lee, B. S. Kong, J. S. Seo and J. W. Choi, *Nano Lett.*, 2012, 12, 802-807.
9. Q. Zhang, W. Zhang, W. Wan, Y. Cui and E. Wang, *Nano Lett.*, 2010, 10, 3243-3249.
10. M. Pharr, K. Zhao, X. Wang, Z. Suo and J. J. Vlassak, *Nano Lett.*, 2012, 12, 5039-5047.
11. K. Fu, O. Yildiz, H. Bhanushali, Y. Wang, K. Stano, L. Xue, X. Zhang and P. D. Bradford, *Adv. Mater.*, 2013, 25, 5109-5114.
12. K. Fu, Y. Lu, M. Dirican, C. Chen, M. Yanilmaz, Q. Shi, P. D. Bradford and X. Zhang, *Nanoscale*, 2014.
13. B. Wang, X. Li, X. Zhang, B. Luo, M. Jin, M. Liang, S. A. Dayeh, S. Picraux and L. Zhi, *ACS Nano*, 2013, 7, 1437-1445.
14. L.-F. Cui, Y. Yang, C.-M. Hsu and Y. Cui, *Nano Lett.*, 2009, 9, 3370-3374.
15. K. Fu, L. Xue, O. Yildiz, S. Li, H. Lee, Y. Li, G. Xu, L. Zhou, P. D. Bradford and X. Zhang, *Nano Energy*, 2013, 2, 976-986.
16. L. Ji and X. Zhang, *Carbon*, 2009, 47, 3219-3226.
17. Y. Li, B. Guo, L. Ji, Z. Lin, G. Xu, Y. Liang, S. Zhang, O. Toprakci, Y. Hu, M. Alcoutlabi and X. Zhang, *Carbon*, 2013, 51, 185-194.

18. M. Dirican, M. Yanilmaz, K. Fu, O. Yildiz, H. Kizil, Y. Hu and X. Zhang, *Journal of The Electrochem. Soc.*, 2014, 161, A2197-A2203.
19. J. Xie, X. Yang, S. Zhou and D. Wang, *ACS Nano*, 2011, 5, 9225-9231.
20. Z. Lin, L. Ji and X. Zhang, *Mater. Lett.*, 2009, 63, 2115-2118.
21. T. Pirzada, S. A. Arvidson, C. D. Saquing, S. S. Shah and S. A. Khan, *Langmuir: ACS J. Surf. Colloids*, 2012, 28, 5834-5844.
22. H. S. Choi, J. G. Lee, H. Y. Lee, S. W. Kim and C. R. Park, *Electrochim. Acta*, 2010, 56, 790-796.
23. J. Xiao, W. Xu, D. Wang, D. Choi, W. Wang, X. Li, G. L. Graff, J. Liu and J.-G. Zhang, *J. Electrochem. Soc.*, 2010, 157, A1047.
24. Y.-S. Ding, W.-N. Li, S. Iaconetti, X.-F. Shen, J. DiCarlo, F. S. Galasso and S. L. Suib, *Surf. Coat. Technol.*, 2006, 200, 3041-3048.
25. L. Su, Y. Jing and Z. Zhou, *Nanoscale*, 2011, 3, 3967-3983.
26. C. Meier, S. Lüttjohann, V. G. Kravets, H. Nienhaus, A. Lorke and H. Wiggers, *Physica E: Low-dimensional Systems and Nanostructures*, 2006, 32, 155-158.
27. Z. Li, W. Gao, A. Meng, Z. Geng and L. Gao, *J. Phys. Chem. C*, 2008, 113, 91-96.
28. Y. Yao, J. Zhang, L. Xue, T. Huang and A. Yu, *J. Power Sources*, 2011, 196, 10240-10243.
29. J. Wang, H. Zhao, J. He, C. Wang and J. Wang, *J. Power Sources*, 2011, 196, 4811-4815.
30. H. Wu, G. Chan, J. W. Choi, Y. Yao, M. T. McDowell, S. W. Lee, A. Jackson, Y. Yang, L. Hu and Y. Cui, *Nat. Nanotechnol.*, 2012, 7, 310-315.
31. B.-C. Yu, Y. Hwa, C.-M. Park, J.-H. Kim and H.-J. Sohn, *RSC Adv.*, 2013, 3, 9408-9413.

## Figure Captions

- Figure 1.** Schematic illustration of the fabrication process of electrospun Si@PAN nanofibers, Si@C nanofibers, and Si@C-SiO<sub>2</sub> nanofibers.
- Figure 2.** SEM images of Si@C nanofiber composite (A) and Si@C-SiO<sub>2</sub> nanofiber composites with different coating times: (B) 0.5 h, (C) 1 h, and (D) 2h.
- Figure 3.** TEM images of Si@C nanofiber composite (A) and Si@C-SiO<sub>2</sub> nanofiber composites with different coating times: (B) 0.5 h, (C) 1 h, and (D) 2h.
- Figure 4.** High-magnification TEM image of Si@C nanofiber composite (A) and Si@C-SiO<sub>2</sub> nanofiber composites with different coating times: (B) 0.5 h, (C) 1 h, and (D) 2h.
- Figure 5.** FTIR spectra of Si@C nanofiber composite (1) and Si@C-SiO<sub>2</sub> nanofiber composites with different coating times: (2) 0.5 h, (3) 1 h, and (4) 2h.
- Figure 6.** WAXD patterns of Si@C nanofiber composite (1) and Si@C-SiO<sub>2</sub> nanofiber composites with different coating times: (2) 0.5 h, (3) 1 h, and (4) 2h.
- Figure 7.** Raman spectra of Si@C nanofiber composite (1) and Si@C-SiO<sub>2</sub> nanofiber composites with different coating times: (2) 0.5 h, (3) 1 h, and (4) 2h.

- Figure 8.** Galvanostatic charge-discharge profiles of Si@C nanofiber composite (A) and Si@C-SiO<sub>2</sub> nanofiber composites with different coating times: (B) 0.5 h, (C) 1 h, and (D) 2h.
- Figure 9.** Cycling performance (A) and coulombic efficiencies (B) of Si@C nanofiber composite and Si@C-SiO<sub>2</sub> nanofiber composites with different coating times: 0.5 h, 1 h, and 2h.
- Figure 10.** Coulombic efficiencies of Si@C nanofiber composite and Si@C-SiO<sub>2</sub> nanofiber composites with different coating times: 0.5 h, 1 h, and 2h with a cutoff voltage window of 0.01 and 1.0 V.
- Figure 11.** Rate capability of Si@C-SiO<sub>2</sub> nanofiber composite with 0.5 h coating time cycled at different current densities.
- Figure 12.** TEM images of cycled Si@C nanofiber composite (A) and Si@C-SiO<sub>2</sub> nanofiber composites with different coating times: (B) 0.5 h, (C) 1 h, and (D) 2h after 50 cycles.

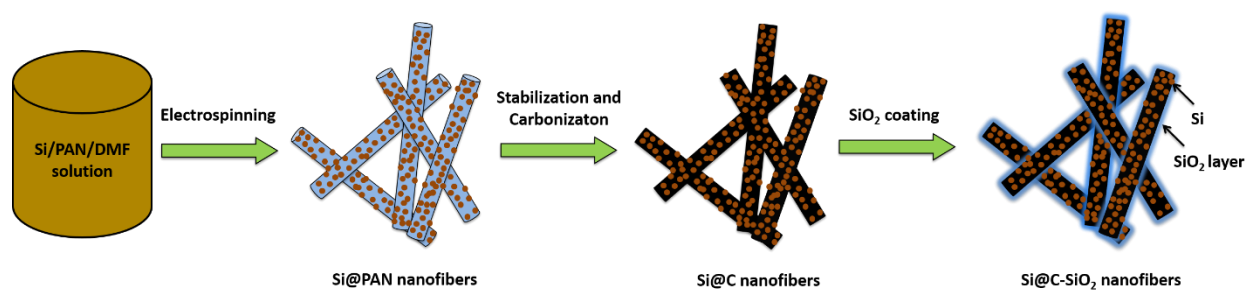


**Figure 1.** Schematic illustration of the fabrication process of electrospun Si@PAN nanofibers, Si@C nanofibers, and Si@C-SiO<sub>2</sub> nanofibers.

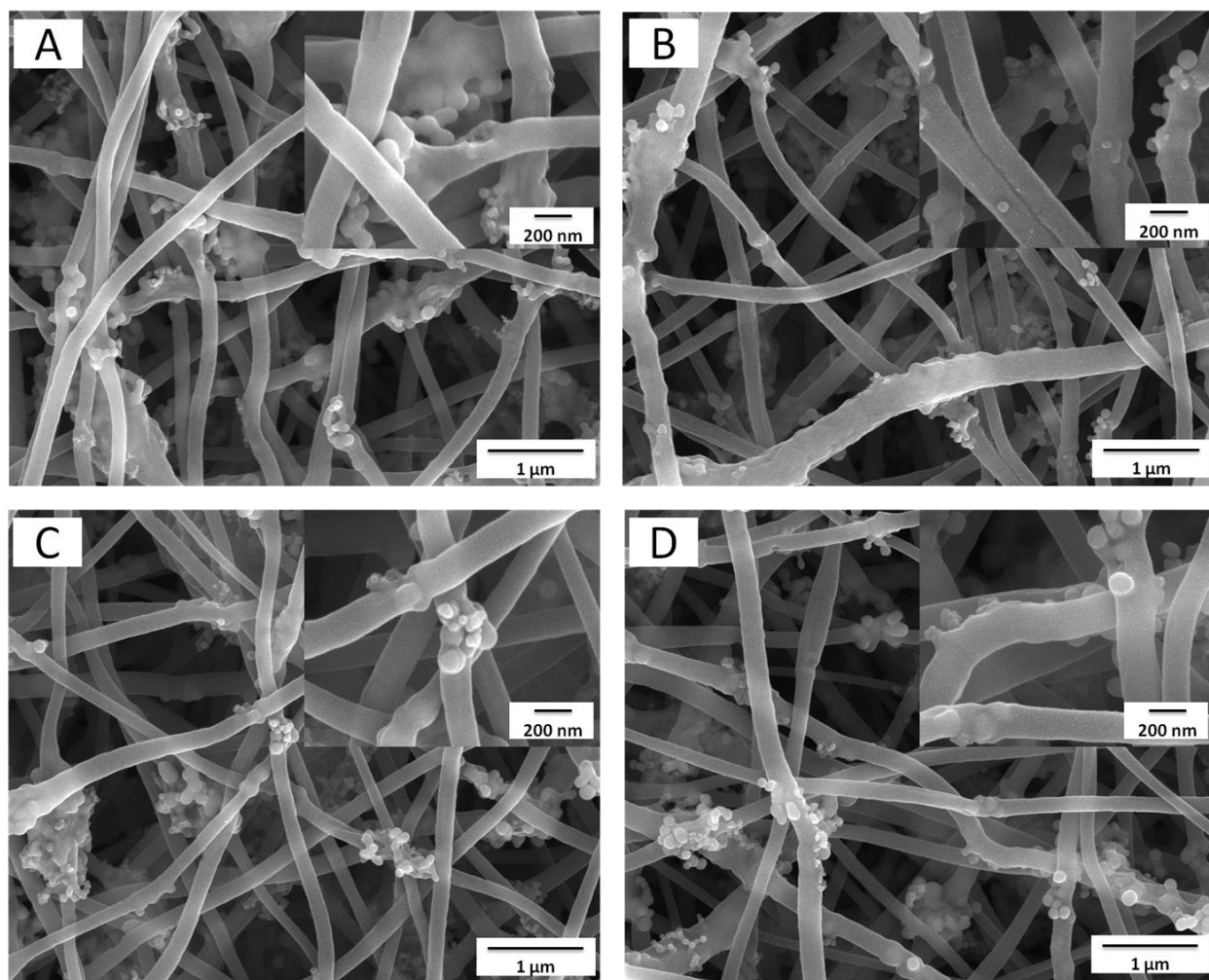


**Figure 2.** SEM images of Si@C nanofiber composite (A) and Si@C-SiO<sub>2</sub> nanofiber composites with different coating times: (B) 0.5 h, (C) 1 h, and (D) 2h.

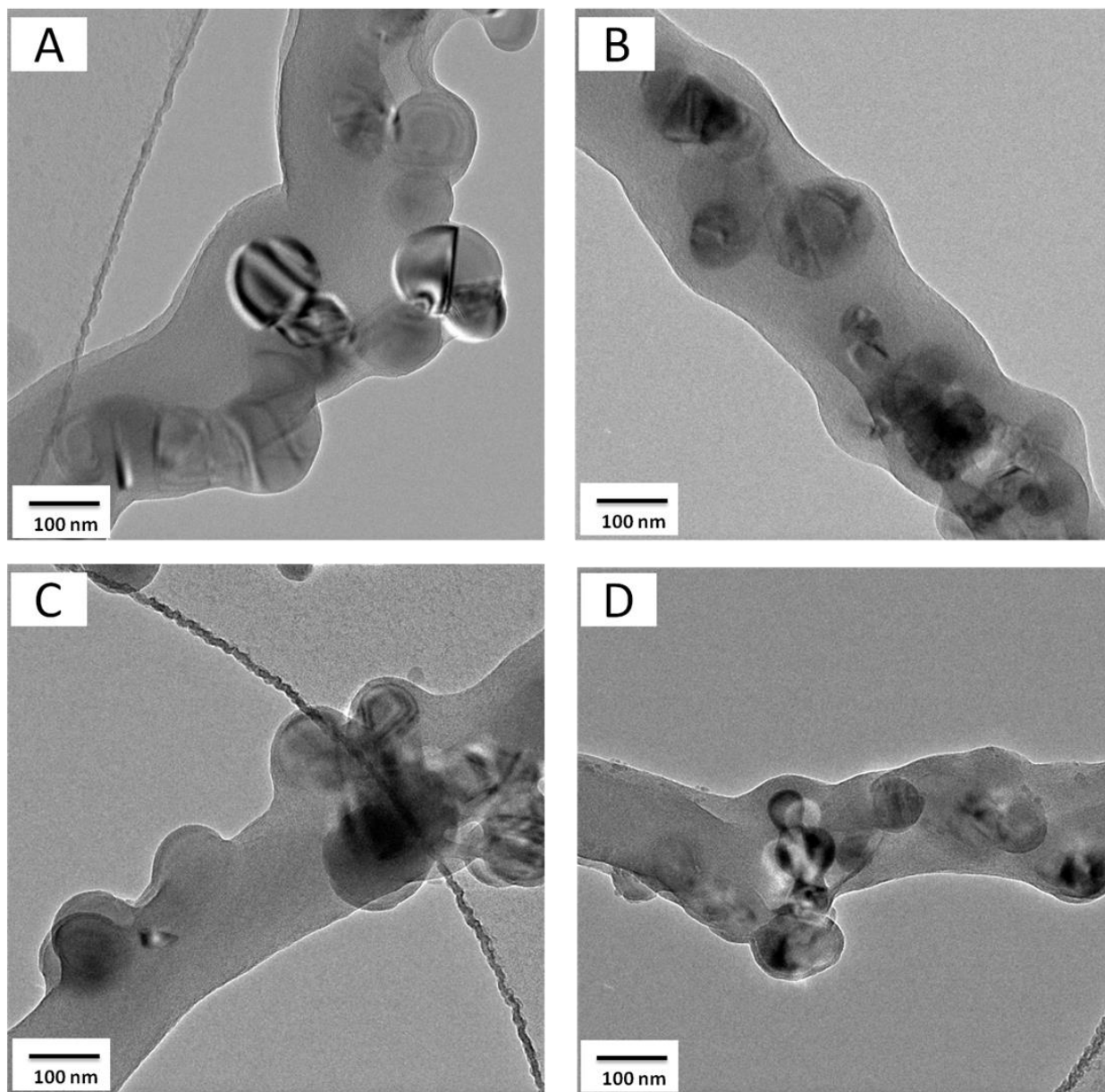


**Figure 3.** TEM images of Si@C nanofiber composite (A) and Si@C-SiO<sub>2</sub> nanofiber composites with different coating times: (B) 0.5 h, (C) 1 h, and (D) 2h.

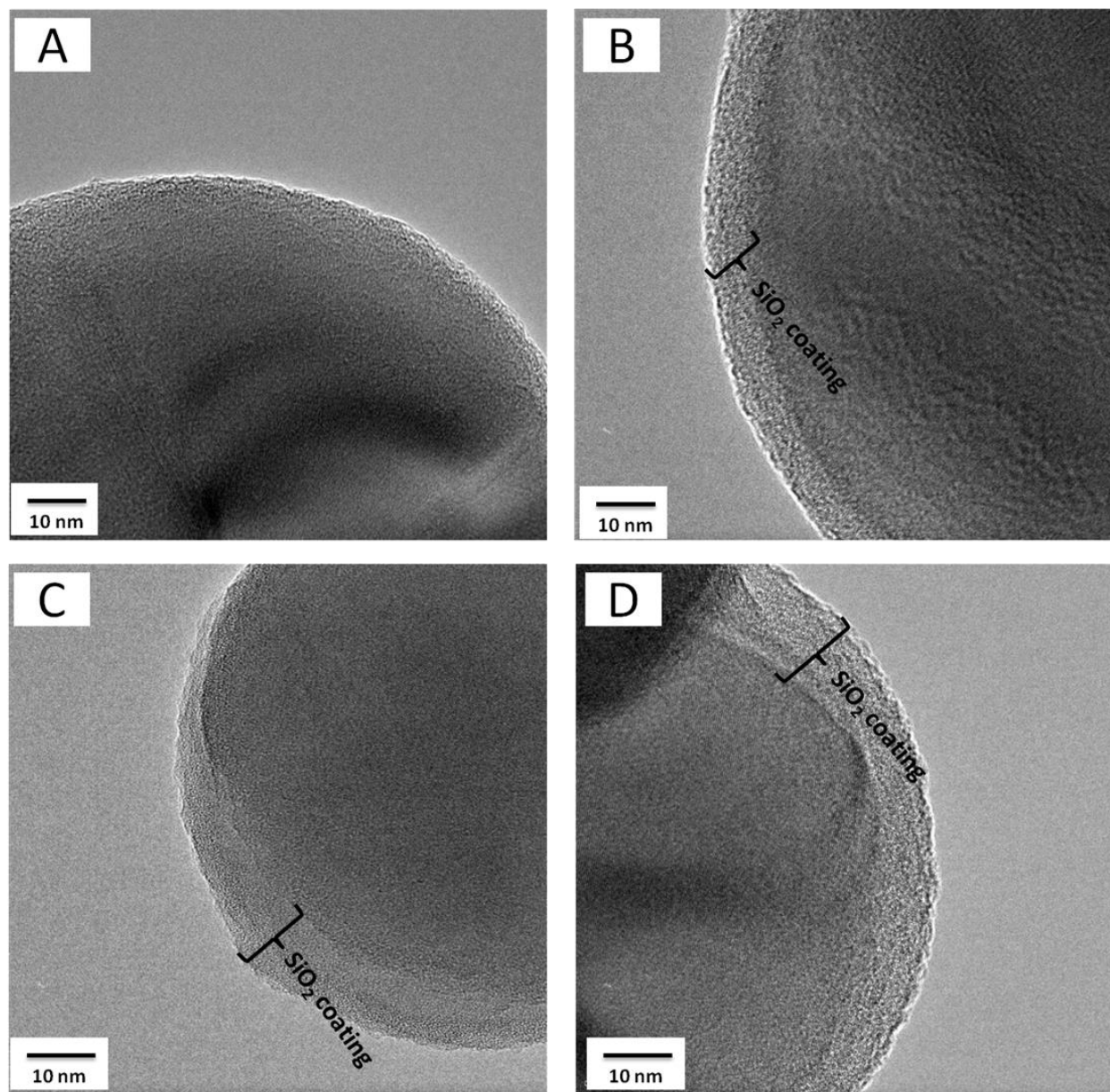


**Figure 4.** High-magnification TEM images of Si@C nanofiber composite (A) and Si@C-SiO<sub>2</sub> nanofiber composites with different coating times: (B) 0.5 h, (C) 1 h, and (D) 2h.

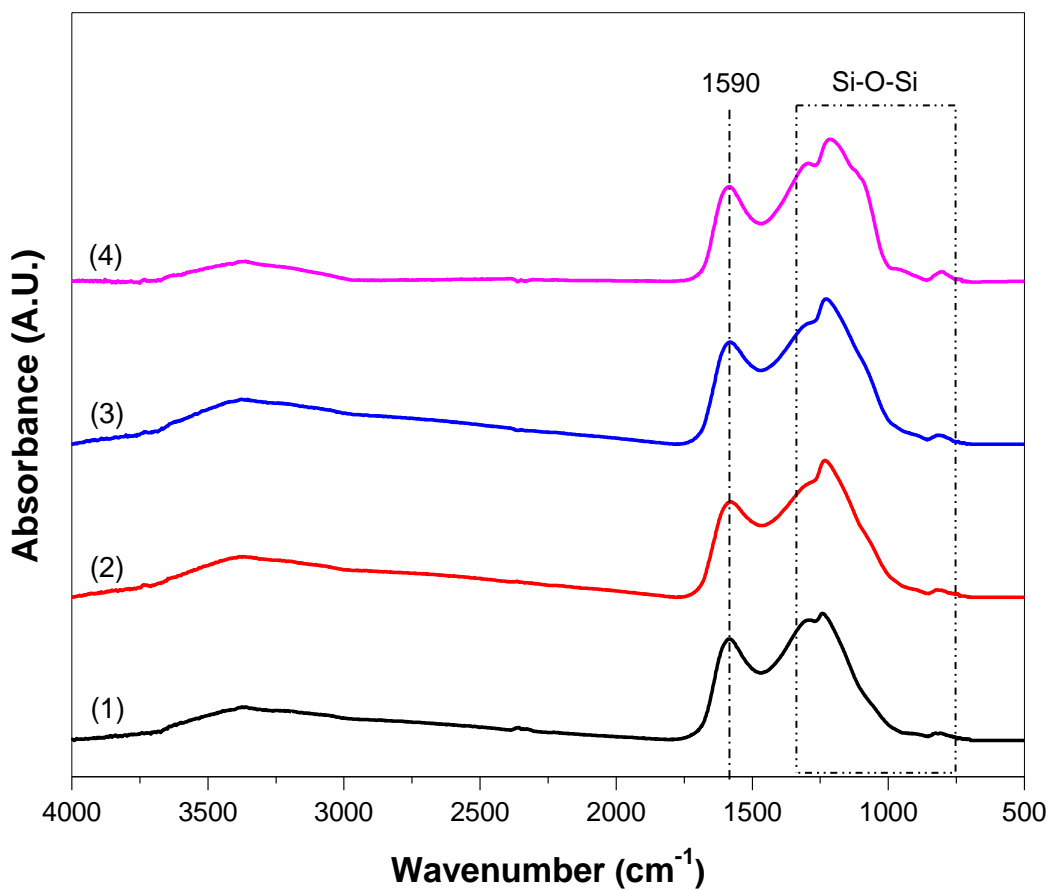


**Figure 5.** FTIR spectra of Si@C nanofiber composite (1) and Si@C-SiO<sub>2</sub> nanofiber composites with different coating times: (2) 0.5 h, (3) 1 h, and (4) 2h.

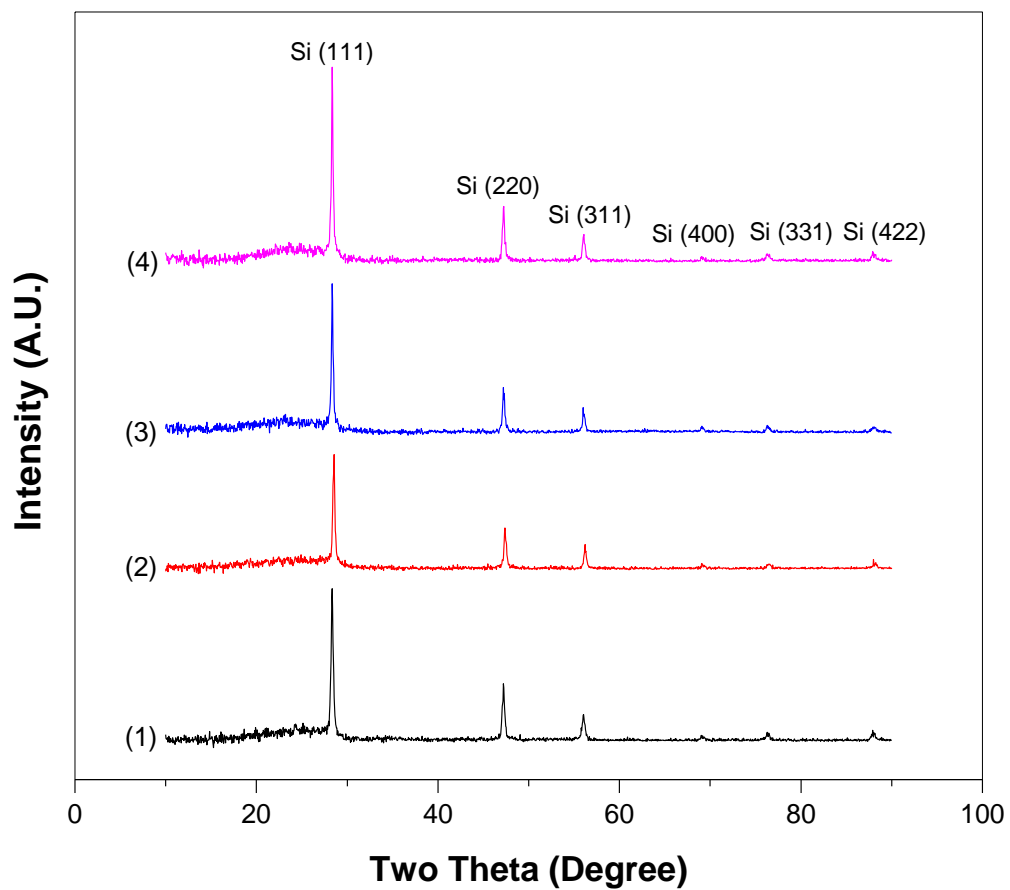


**Figure 6.** WAXD patterns of Si@C nanofiber composite (1) and Si@C-SiO<sub>2</sub> nanofiber composites with different coating times: (2) 0.5 h, (3) 1 h, and (4) 2h.

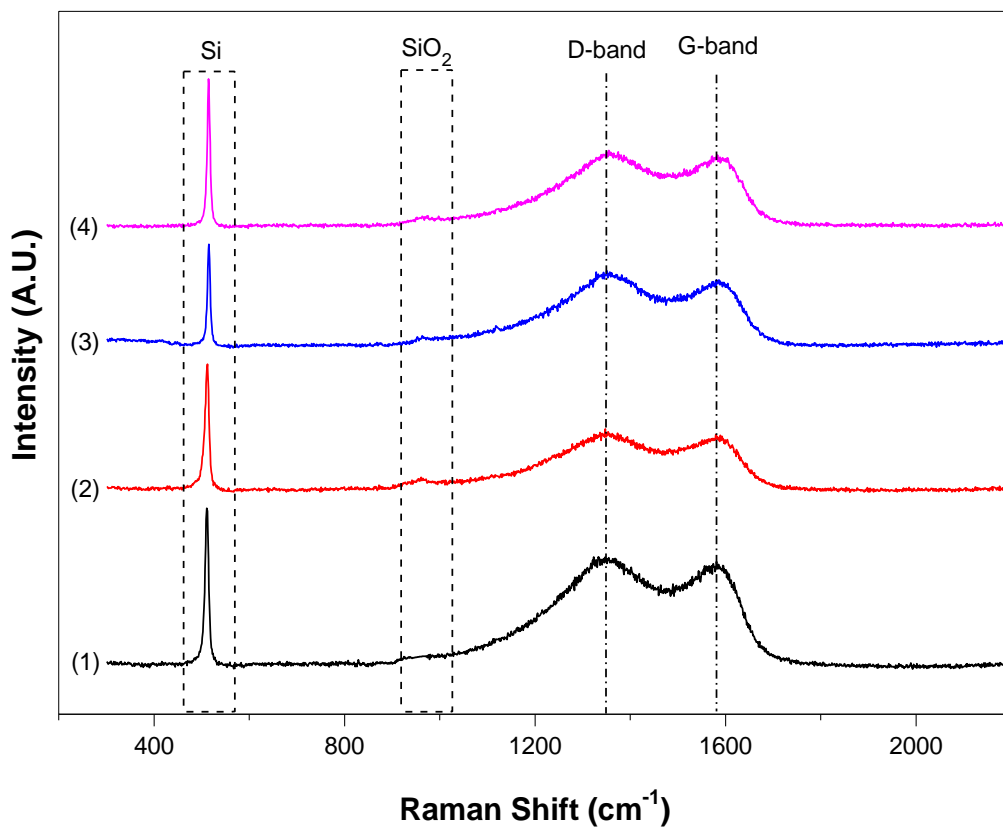


**Figure 7.** Raman spectra of Si@C nanofiber composite (1) and Si@C-SiO<sub>2</sub> nanofiber composites with different coating times: (2) 0.5 h, (3) 1 h, and (4) 2h.

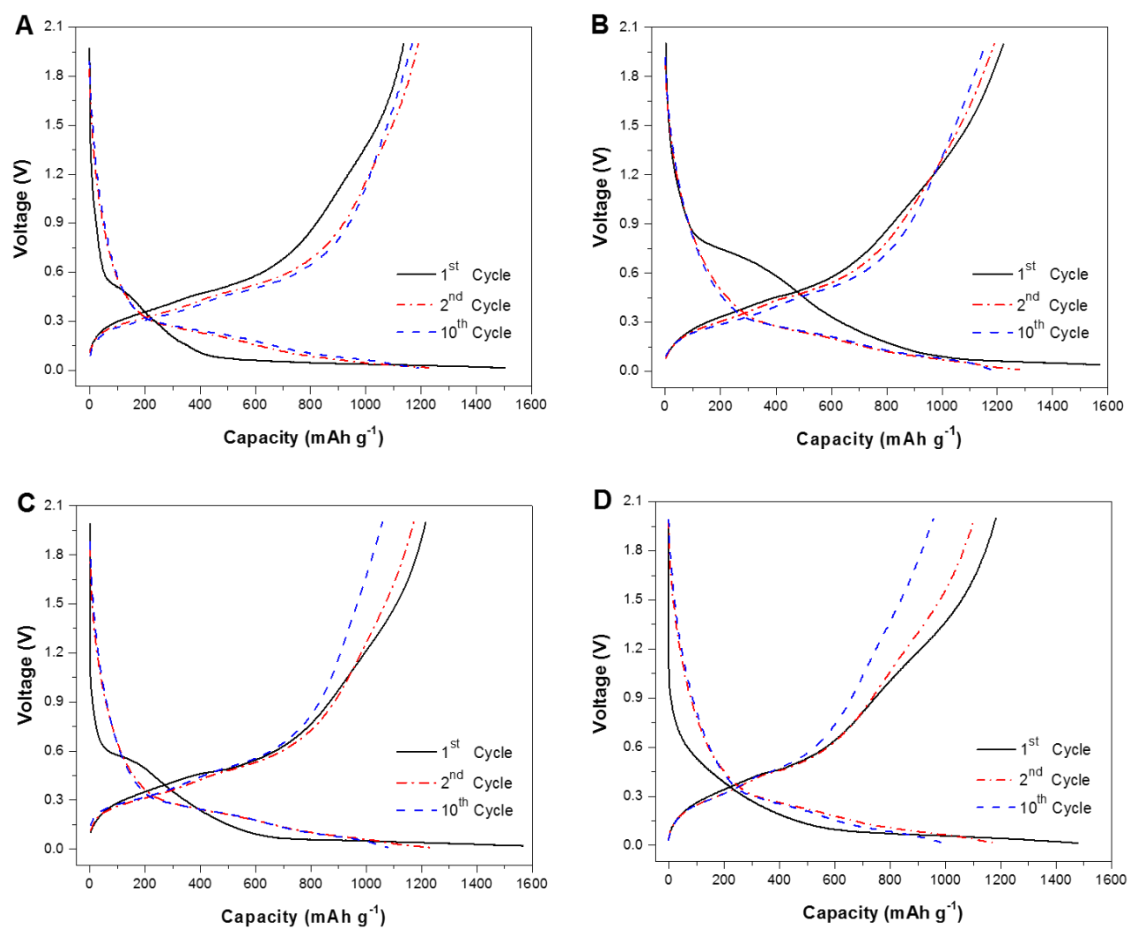


**Figure 8.** Galvanostatic charge-discharge profiles of Si@C nanofiber composite (A) and Si@C-SiO<sub>2</sub> nanofiber composites with different coating times: (B) 0.5 h, (C) 1 h, and (D) 2h.

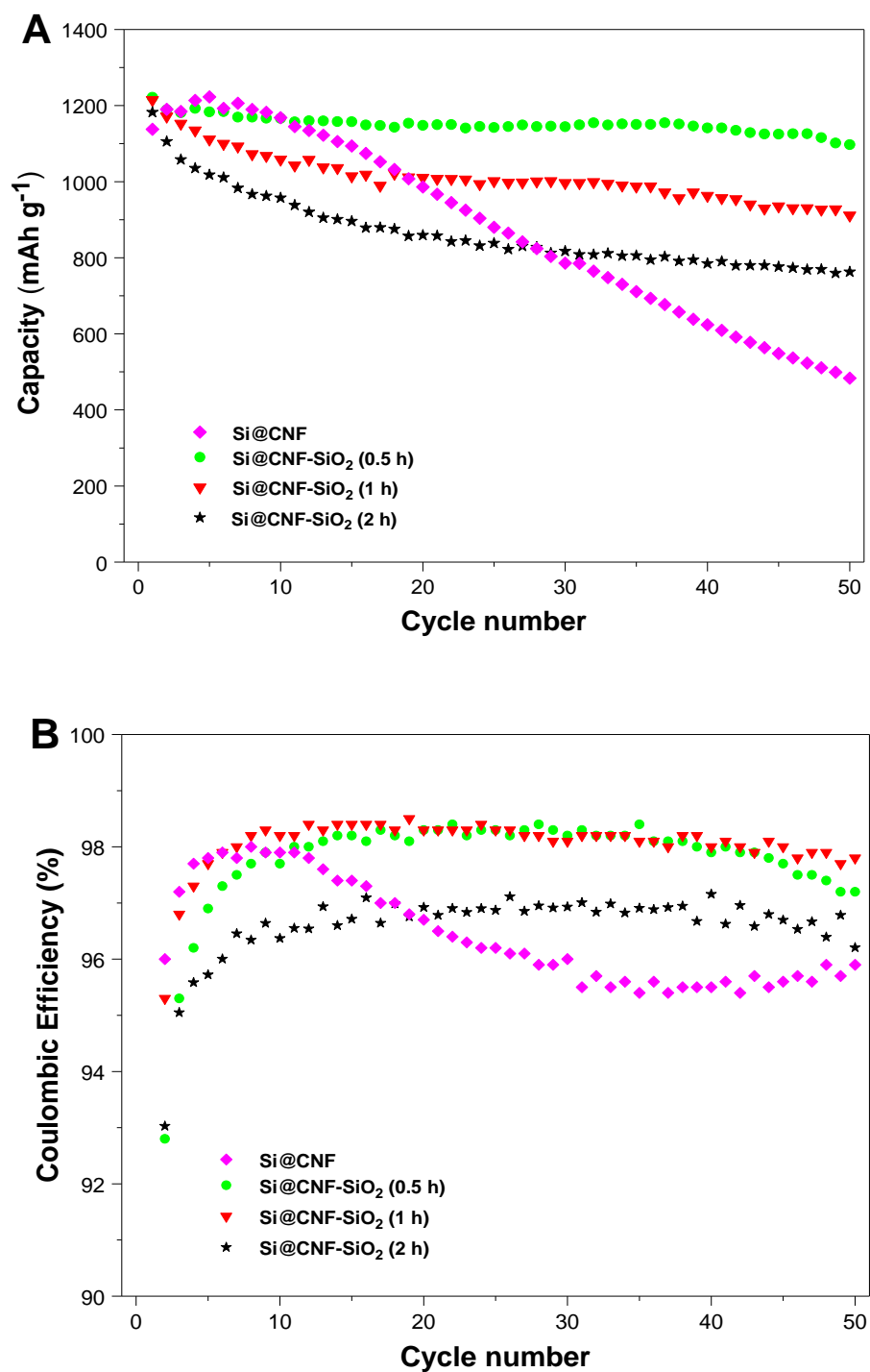


**Figure 9.** Cycling performance (A) and coulombic efficiencies (B) of Si@C nanofiber composite and Si@C-SiO<sub>2</sub> nanofiber composites with different coating times: 0.5 h, 1 h, and 2h.

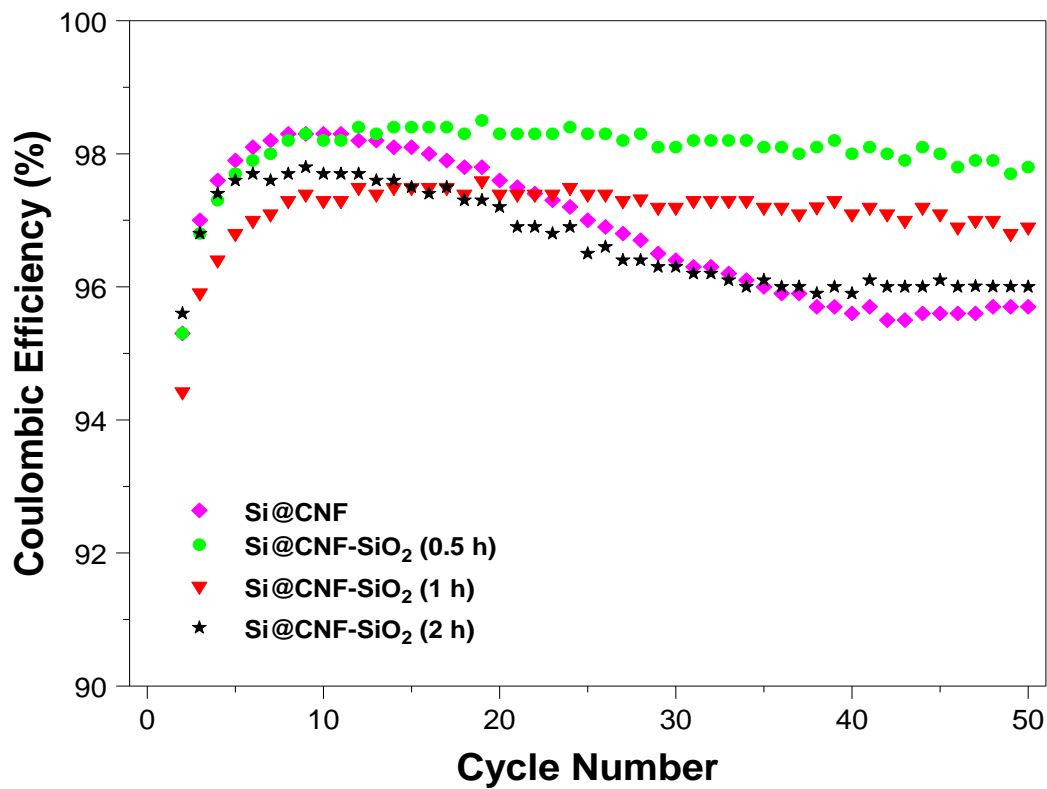


**Figure 10.** Coulombic efficiencies of Si@C nanofiber composite and Si@C-SiO<sub>2</sub> nanofiber composites with different coating times: 0.5 h, 1 h, and 2h with a cutoff voltage window of 0.01 and 1.0 V.

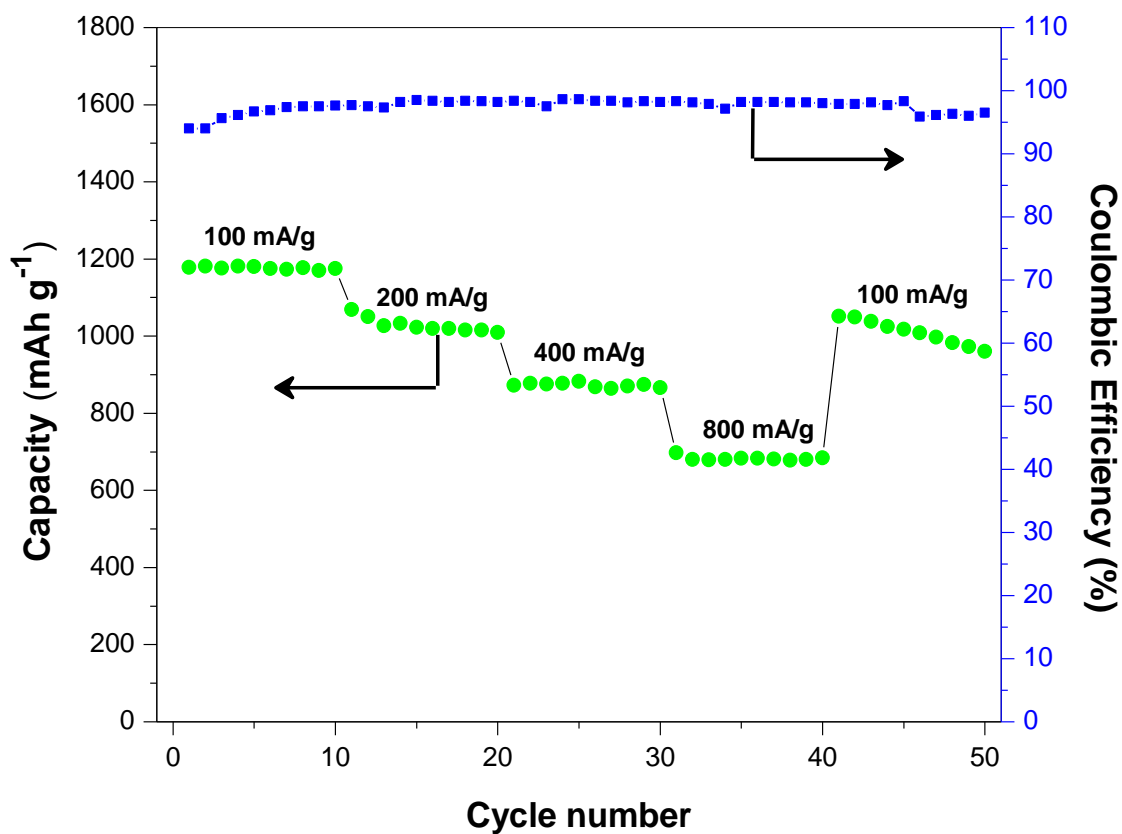


**Figure 11.** Rate capability of Si@C-SiO<sub>2</sub> nanofiber composite with 0.5 h coating time cycled at different current densities.

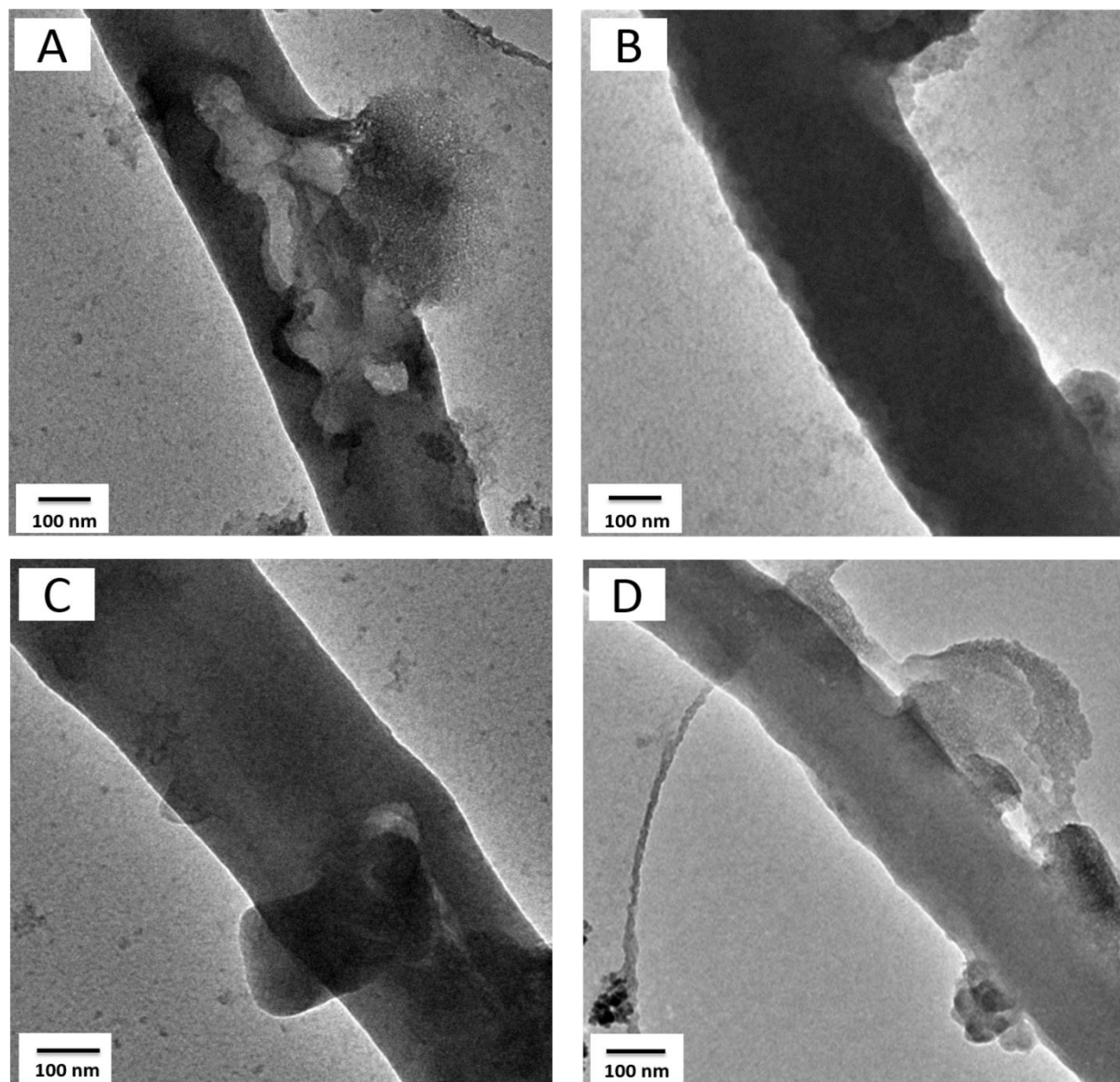


**Figure 12.** TEM images of cycled Si@C nanofiber composite (A) and Si@C-SiO<sub>2</sub> nanofiber composites with different coating times: (B) 0.5 h, (C) 1 h, and (D) 2h after 50 cycles.